

SOL-GEL SYNTHESIS AND CHARACTERIZATIONS OF In-DOPED ZnO NANOPARTICLES

J. EL GHOUL^{a,b,*}, L. EL MIR^a

^a *Imam Mohammad Ibn Saud Islamic University (IMSIU), College of Sciences, Department of Physics, Riyadh 11623, Saudi Arabia.*

^b *Laboratory of Physics of Materials and Nanomaterials Applied at Environment (LaPhyMNE), Faculty of Sciences, Gabes University, 6072 Gabes, Tunisia*

Indium doped ZnO (In-ZnO) nanoparticles by a sol-gel processing technique has been synthesized for a concentration of In ranging from 0 to 5%. The structural and optical properties of ZnO and In-ZnO nanoparticles were characterized by different techniques. The structural study confirms the presence of hexagonal wurtzite phase and indicates the indium incorporation of In³⁺ ions at the Zn²⁺ sites. However, the optical study was shown a high absorption in the UV range and an important reflectance in the visible range. The optical band gap of In-ZnO samples were varied between 3.16 and 3.22 eV. The aim of this work is to study the effect of indium doping on the structural, morphological and optical properties of ZnO nanoparticles.

(Received June 15, 2019; Accepted November 7, 2019)

Keywords: Sol-gel process, In-doped ZnO, Structural properties, Optical materials

1. Introduction

In recent years, great efforts have been devoted to the doping of semiconductor nanomaterials. Many studies on Transparent Conductive Oxides (TCOs) have brought an important interest in nanotechnology because they may have the dual properties of having good transmittance in the visible light region and high electrical conductivity [1]. These characteristics depend on the nature, the number and the atomic arrangement of the metal cations in the crystalline oxide structure, the morphology of the nanomaterials and the presence of intrinsic (oxygen vacancies and interstitial metal) or extrinsic (doping) defects. Currently, the dominant TCOs are SnO₂, TiO₂, ZnO and Indium Tin Oxide (ITO). Zinc oxide is considered today as the promising key for several nanotechnology applications. In particular, it offers good prospects as a transparent conductive oxide when doped with several types of dopants such as indium (In) [2], ytterbium (Yb)[3], molybdenum (Mo) [4] and vanadium (V) [5]. ZnO nanostructures with different morphologies have particular properties, so there are very intense interests have been devoted to the synthesis of ZnO with various morphologies such as nanowires, nanorods and nanobelts. In fact, ZnO as a semiconductor has a wide band gap (3.3 eV), a large exciton binding energy of 60 meV at room temperature (RT) [6-7], abundant in nature and environmentally friendly; these characteristics make this material attractive for many applications such as solar cells, optical coatings, photocatalysts, antibacterial activities, electrical devices, active medium in UV semiconductor lasers and in gas sensors, there by allowing faster detection and response [8-13]. ZnO nanomaterials can be doped with transition metals (Co, Fe, Mn, Ni, etc.) [14-17] or with poor metals (Al, Ga, In, Sn, etc.) [18-21], synthesized by several techniques (PLD, sputtering) and chemical techniques (spin-coating, pyrolysis spray, sol-gel, etc.). In this field, an In-ZnO material has been used in the detection of various high concentrations of VOCs [22],

* Corresponding author: Jaber.Elghoul@fsg.rnu.tn

solar cells [23] and photocatalysts [24]. Focus has been given on the application of In-ZnO in the dye sensitized solar cells (DSSCs). The incorporation of indium into ZnO NPs allows for the inhibition of the recombination of photo-generated electron and holes, collecting more charge and enhancing the conversion efficiency values [25]. Kim et al. [26] synthesized the In-doped ZnO materials via the sol-gel route, they found that when Indium dopant was added to ZnO materials at 0.5 mol%, it increased the carrier concentration, therefore reducing the resistivity of the materials. Zhu et al. [27] elaborated the In-doped ZnO nanoparticles by renovating hybrid induction and laser heating (HILH), with different mole ratios and they found that by increasing the dopant concentration of In in ZnO, its resistance increased while its sensitivity decreases.

Therefore, in this work, we describe our approach for synthesis ZnO nanoparticles and study the influence of indium doping with different concentrations on the structural, morphological and optical properties of ZnO nanoparticles.

2. Experimental details

2.1. Sample preparation

Pure and Indium doped ZnO nanoparticles with various concentration of indium were prepared by a sol-gel method as follow: 16 g of zinc acetate dehydrate [$\text{ZnC}_4\text{H}_6\text{O}_4 \cdot 2\text{H}_2\text{O}$] (Sigma Aldrich $\geq 99\%$ purity) as a host precursor was dissolved in a 112 ml methanol (CH_3OH) as solvent. After 10 min of magnetic stirring at room temperature, indium chloride (InCl_3 ; Sigma Aldrich 98% purity) was added as the indium dopant precursor with different concentrations ranging from 0 to 5%, and continue with magnetic stirring until the total dissolution of the precursors. After, the resultant solution was placed in an autoclave by adding a 220 ml ethanol ($\text{C}_2\text{H}_5\text{OH}$) for drying in the supercritical conditions of the latter, using the J. El Ghoul et al. protocol [28].

2.2. Characterisation techniques

The effect of indium concentrations on the crystalline phase of the obtained nanoparticles was monitored with the help of Bruker D5005 powder X-ray diffractometer using $\text{CuK}\alpha$ ($\lambda=1.5418 \text{ \AA}$). The recorded X-ray diffraction patterns of ZnO and In-ZO were investigated in an angle (2θ) ranging from 20° to 70° with a step of 0.02° . X-ray photoelectron spectroscopy (XPS: PHI-5702) was used to investigate the chemical and the surface binding energy states of In-doped ZnO samples. The synthesized samples were also characterized by using a transmission electron microscope (TEM)(JEM-200 CX) and an haute resolution scanning electron microscope(HRSEM)(JOEL JSM-5310 LV). The composition studies were done by energy dispersive X-ray spectrometry (EDX) that is accompanied by the TEM. The optical-absorption spectra and diffuse reflectance spectra were measured on Shimadzu (UV-3101 PC UV-Vis-NIR) spectrophotometer in the wavelength range of 200-1800 nm. The powder of BaSO_4 was used as a standard for the optical measurements.

3. Results and discussion

X-ray diffraction analysis was carried out to study the crystal phases of ZnO and In-ZnO nanoparticles. Fig. 1 shows the XRD patterns of In-ZnO nanoparticles with different indium doping concentrations. The results indicate the formation of hexagonal wurtzite phase of ZnO [29], matched well with space group $P6_3mc$ (No. 186) (JCPDS No. 36-1451). It is clear in fig.(1) that, XRD patterns of different doping concentrations are similar to XRD pattern of undoped ZnO. The values of lattice constants at room-temperature of doped In-ZnO materials are agreed with hexagonal polycrystalline wurtzite structure of ZnO ($a = 3.249 \text{ \AA}$ and $c = 5.206 \text{ \AA}$ [30]. This implies that the doping of In-ZnO has retains the same crystal structure of ZnO. In addition, when the

doping rate reaches up to 4%, a secondary phase of low intensity was observed corresponds to In_2O_3 and probably due to a nucleation favored by indium with a high concentration of doping [31].

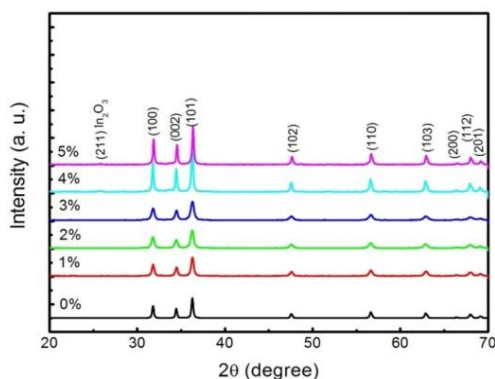


Fig. 1. X-ray diffraction patterns of undoped ZnO and indium doped.

The average crystallite size D was evaluated using the Debye-Scherrer formula as given [32]:

$$D = \frac{0.9\lambda}{B \cos \theta_B} \quad (1)$$

Where λ is the X-ray wavelength (1.5418 \AA), θ_B is the maximum of the Bragg diffraction peak and B is the fullwidth at half maximum ($FWHM$) of diffracted peaks measured in radians.

By increasing the doping concentration of In from 1 to 3%, the full width at half-maximum ($FWHM$) increases, however, the doping of 4 and 5%, peak intensity increases and the peaks become finer than the other samples. This is an indicator of a change in the unit cell of the hexagonal structure due to the substitution of Zn^{2+} by In^{3+} . The crystallite size of undoped ZnO and In-ZnO of different doping concentrations have been calculated and summarized in Table (I). The size of undoped and In-ZnO nanoparticles crystallites varies between 22 and 40 nm. Wang et al. [33] prepared the monodisperse In-doped ZnO nanomaterials by using a one-step ester elimination reaction based on alcoholysis of metal carboxylate salts, and found that the reduction in the particle size implies that the indium species play an important role in the fabrication of the nanomaterials.

The XPS analysis was used for further evaluation of purity and the chemical composition of the $\text{In}_{3\%}\text{-ZnO}$ and measured spectra are shown in Fig. 2.a. The XPS survey scan revealed the presence of the binding energy of the main constituents of the ZnO crystal lattice before and after In^{3+} doping, in addition the adventitious C1s carbon peak was detected for both samples. The asymmetric peak O-1s was observed in the region (529-533 eV) at about 532 eV and there are various discussions on the oxygen core level spectrum.

By concerning the case of ZnO:Al materials, an oxygen core level shows two spectral components; One component at $531.25 \pm 0.20 \text{ eV}$ has been related to O^{2-} ions in the oxygen-deficient regions within the ZnO structure [34].

The other component at $530.15 \pm 0.15 \text{ eV}$ was estimated to be related with the O^{2-} ions in the wurtzite structure of the hexagonal Zn^{2+} ion array [35]. We note the presence of two peaks centred at 1022 and 1045.2 eV attributed to the spin-orbit coupling of 3/2 ($\text{Zn } 2p_{3/2}$) and 1/2 ($\text{Zn } 2p_{1/2}$), respectively [36-37]. Fig. 2 b shows two peaks which are located at binding energies 452.34 and 444.85 eV corresponding to the

electronic states of In $3d_{3/2}$ and In $3d_{5/2}$, respectively. The difference between these two peaks is 7.49 eV, which corresponding well to the standard value 7.5 eV.

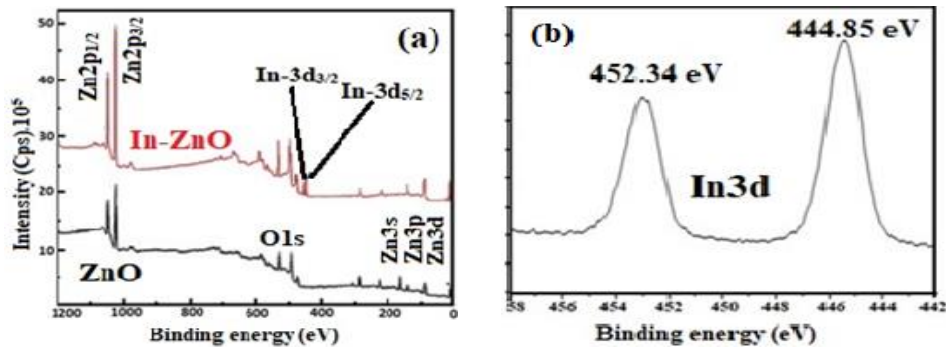


Fig. 2. XPS spectra of nanoparticles $In_{3\%}\text{-ZnO}$.

The SEM observation in Fig. 3 shows that, ZnO crystallites are hexagonal in its shape and reveal an increase in its size with increasing doping concentrations.

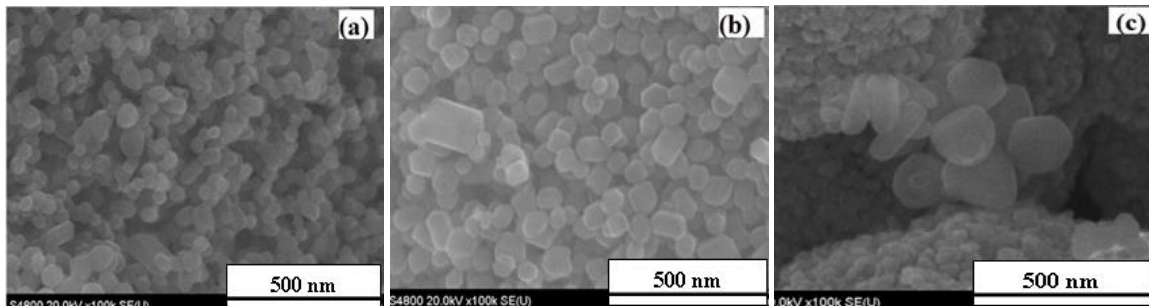


Fig. 3. HRSEM images of the powder: (a) $In_{1\%}\text{-ZnO}$, (b) $In_{3\%}\text{-ZnO}$, and (c) $In_{5\%}\text{-ZnO}$.

Fig.4 shows the TEM images of In-ZnO nanopowders. It is clear that, In-ZO nanoparticles are fine and has hexagonal shape at low indium concentration and shifted to a cylindrical prismatic structure at high concentration with diameter ranging from 23 to 44nm.

Fig.4c, clearly showed randomly scattered diffraction spots along with ring patterns, which reveal that pure as well as In doped ZnO nano-powders consist of single as well as poly-crystalline nanocrystallites. The observed diffraction spots and rings are indexed with the help of bulk ZnO JCPDS card36-1451 data, as shown in Fig.4.

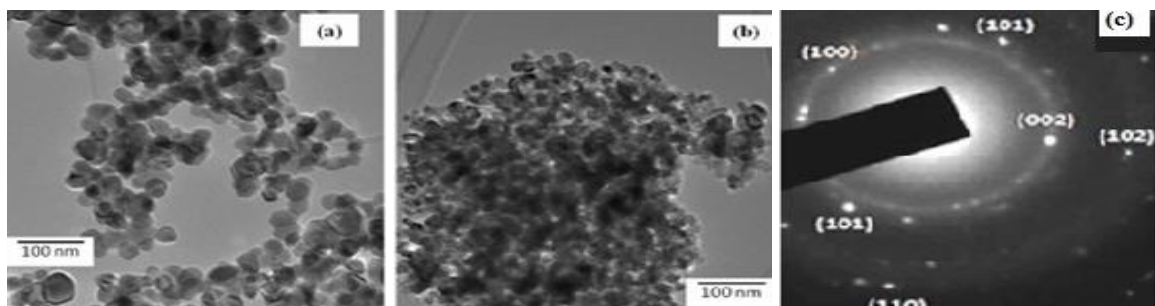


Fig. 4. TEM images: (a) ZnO , (b) $In_{3\%}\text{-ZnO}$, and (c) SAED pattern of $In_{3\%}\text{-ZnO}$.

In order to investigate the optical properties and band gap, the absorbance spectra of the samples was carried out by UV-Vis spectrophotometer. The reflectance spectra of In-ZO nanoparticles at different concentrations of indium in UV and visible range are presented in Fig. 5.

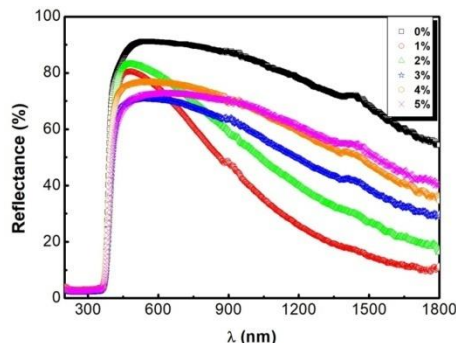


Fig. 5. UV-Vis-NIR reflectance spectra of In-ZO nanoparticles for different Indium doping concentrations.

It is clear that, the reflectance are varied at different doping concentrations from 3% to 4% in the UV range, which shows that absorption is the highest in this region. In contrast, the reflectances are varied between 65% and 80% in the visible light region, which prove that the optical diffusion power of this type of material is quite important in this range.

The band gap energies have been estimated by using the method of the first derivative of the reflectance ($dR/d\lambda$) [38, 39]. The variation spectrum of the first derivative of the reflectance ($dR/d\lambda$) versus wavelength (λ) for $\text{In}_{4\%}\text{-ZnO}$ nanoparticles is shown inset in Fig. 6.

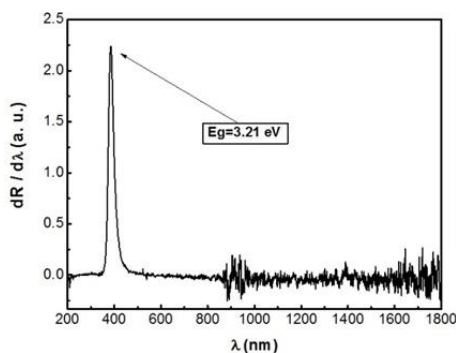


Fig. 6. Spectrum of first derivative of reflectance of $\text{In}_{4\%}\text{-ZnO}$ nanoparticles.

We found that, the estimated values of the band gap energy from this method are summarized in Table 1. It has been reported that the In^{3+} ions create a donor level below the conduction band inducing a curvature at the edge of the band, thus reducing the width of the band gap [40]. In addition, the decreases in the gap energy can be attributed to the fact that the indium atoms are not completely absorbed by the host matrix of ZnO. So, some indium atoms are positioned on the surface of the ZnO, giving rise to allowed states near the conduction band in the band gap. Similar results have been reported for Sn-doped ZnO [41] and Al-doped ZnO [42], where the oxides SnO_2 and Al_2O_3 appear on the surfaces of the doped ZnO. For high concentrations of doping, the slight increase in gap energy may be due to the appearance of the secondary phase In_2O_3 whose gap energy varies between 3.5 and 3.7 eV [43], which it confirmed by X-ray diffraction.

Table 1. Lattice parameters values the crystallites size and band gap energies of the samples.

In (at. %)	a (101)	c (002)	D (nm)	Eg (eV)
0	3.250	5.206	33	3.22
1	3.249	5.203	27	3.16
2	3.251	5.208	24	3.18
3	3.250	5.205	22	3.19
4	3.251	5.208	40	3.21
5	3.242	5.194	39	3.18

4. Conclusions

In summary, undoped ZnO and In-ZO were synthesized by a sol-gel technique. The structural study of XRD indicated that the synthesized undoped and In-ZO nanoparticles are crystallized in a hexagonal wurtzite structure with crystallite size varies between 22 and 40 nm. According to TEM and HRSEM analysis, the shape of crystallites was transformed from a hexagonal to cylindrical prismatic with increasing in its size as indium concentration increased.

The optical study of ZnO and In-ZO samples reveals the presence of the intense absorption in the UV range as well as the significant reflectance in the visible and infrared region where these results are agreed with the common behaviour of ZnO nanoparticles. The band gap energy of ZnO and In-ZnO were estimated from the variation of the first derivative of the reflectance versus wavelength (λ) and its values are between 3.16 and 3.22 eV where it is in a good agreement with those obtained by the method of the first derivative of the reflectance.

Acknowledgements

The authors extend their appreciation to the Deanship of Academic Research at Imam Mohamed Ibn Saud Islamic University (IMSIU), Riyadh, Kingdom of Saudi Arabia, for funding the work through research project Number 381212, 1438H.

References

- [1] K. Goto, T. Kawashima, N. Tanabe, Sol. Energy Mater. Sol. Cells **90**, 3251 (2006).
- [2] C. Manoharan, G. Pavithra, S. Dhanapandian, P. Dhamodharan, Spectrochim. Acta Part A **149**, 1 (2015).
- [3] G.H. Mhlongo, B.M. Mothudi, K.T. Hillie, H.C. Swart, M.S. Dhlamini, Mater. Lett. **119**, 71 (2015).
- [4] G. Chen, X. Zhao, H. Zhang, F. Liu, Y. Wang, H. Wang, J. Gao, Y. Zhao, W. Li, J. Tao, Superlattices Microstruct **99**, 175 (2016).
- [5] J. El Ghoul, J. Mater. Sci: Mater Electron **27**, 1 (2015).
- [6] L. Yan, C. K. Ong, X.S. Rao, J. Appl. Phys **96**, 508 (2004).
- [7] J. El Ghoul, Bull. Mater. Sci **39**, 7 (2016).
- [8] Ü. Özgür, H. Morkoç, Zinc Oxide Bulk, 1st Edition, Elsevier, Thin Films. Nanostruct, 2006, p. 1.
- [9] R. Razali, A. Khorsand Zak, W.H. A. Majid, M. Darroudi, Ceram. Int. **37**, 3657 (2011).
- [10] P. Sharma, K. Sreenivas, K.V. Rao, J. Appl. Phys **93**, 3963 (2003).
- [11] T. Movlaroooy, J. Magn. Magn. Mater **441**, 139 (2017).
- [12] Y. Dou, F. Wu, C. Mao, L. Fang, S. Guo, M. Zhou, J. Alloys Compd **633**, 408 (2015).
- [13] C.L. Hsu, D.X. Hsu, T.J. Hsueh, S.P. Chang and S.J. Chang, Ceram. Int. **43**, 5434 (2017).
- [14] L. El Mir, Z. Ben Ayadi, H. Rahmouni, J. El Ghoul, K. Djessas, H.J. von Bardeleben, Thin Solid Films **517**, 6007 (2009).
- [15] J. El Ghoul, M. Kraini, O.M. Lemine, J. Mater. Sci. Mater Electron **26**, 2614 (2015).

- [16] K. Omri, J. El Ghoul, O.M.Lemine, M. Bououdina, B. Zhang, L. El Mir, *Superlattices Microstruct* **60**, 139 (2013).
- [17] J. El Ghoul, M. Kraini, L. El Mir, *J. Mater.Sci. Mater Electron***26**, 2555(2015).
- [18] M. Hjiri, L. El Mir, S.G. Leonardi, A. Pistone, L. Mavilia, G. Neri, *Sens. Actuators B* **196**, 413 (2014).
- [19] I. Ghiloufi, J. El Ghoul, A. Modwi, L. El Mir, *Mater. Sci. Semicond. Process***42**, 102 (2016).
- [20] M. Hjiri, R. Dhahri, K. Omri, L. El Mir, S. G. Leonardi, N. Donato, G. Neri, *Mater. Sci. Semicond. Process* **27**, 319 (2014).
- [21] S. Ameen, M.S. Akhtar, H.K. Seo, Y. S. Kim, H.S. Shin, *Chem. Eng. J.***187**, 351 (2012).
- [22] R. Dhahri, M. Hjiri, L. El Mir, H. Alamri, A. Bonavita, D. Iannazzo, S. G. Leonardi, G. Neri, *Adv. Mater. Devices* **2**, 34 (2017).
- [23] R. Menner, M. Cemernjak, S. Paetel, W. Wischmann, *Thin Solids Films***633**, 239 (2017).
- [24] R. Slama, J. El Ghoul, K. Omri, A. Houas, L. El Mir, F. Launay, *J. Mater.Sci. Mater Electron.***27**, 7939 (2016).
- [25] R. K. Chava, M. Kang, *J. Alloys Compd.***692**, 67 (2017).
- [26] S. Kim, C. Kim, J. Na, E. Oh, C. Jeong, S. Lim, *J. Sol-Gel Sci. Technol.***74**, 790 (2015).
- [27] B. L. Zhu, D. W. Zeng, J. Wu, W. L. Song, C. S. Xie, *J. Mater. Sci.- Mater Electron* **14**, 521 (2003).
- [28] J. El Ghoul, C. Barthou, L. El Mir, *SuperlatticesMicrostruct.* **51**, 942(2012).
- [29] J. El Ghoul, C. Barthou, M. Saadoun, L. El Mir, *J. Phys. B* **405**, 597 (2010).
- [30] R. Slama, J. El Ghoul, I. Ghiloufi, K. Omri, L. El Mir, A. Houas, *J Mater Sci: Mater Electron*, **27**, 8146 (2016).
- [31] C.S. Prajapati, P.P. Sahay, *Mater. Sci. Semicond. Process* **16**, 200 (2013).
- [32] J. El Ghoul, N. Bouguila, S. A. Gómez-Lopera, L. El Mir, *SuperlatticesMicrostruct***64**, 451 (2013).
- [33] Qing Ling Wang, Ye Feng Yang, Hai Ping He, Dong Dong Chen, Zhi Zhen Ye, Yi Zheng Jin, *Nanoscale Res. Lett.***5**, 882 (2010).
- [34] John C. C. Fan, John B. Goodenough, *J. Appl. Phys* **48**, 3524 (1997).
- [35] Y.M. Chung, C.S. Moon, M. J. Jung, J.G. Han, *Surf. Coat. Technol.***200**, 936 (2005).
- [36] S.Y. Huang, Q.J. Cheng, S. Xu, D.Y. Wei, H.P. Zhou, J. D. Long, I. Levchenko, K. Ostrikov, *J. Appl. Phys* **111**, 036101 (2012).
- [37] O. Lupan, G.A. Emelchenko, V.V. Ursaki, G. Chai, A.N. Redkin, A.N. Gruzintsev, I.M. Tiginyanu, L. Chow, L.K. Ono, B. Roldan Cuenya, H. Heinrich, E.E. Yakimov, *Mater. Res. Bull* **45**, 1026 (2010).
- [38] G. Riveros, H Gomez, R. Henríquez, R. Sshrebler, R. Cordova, R. E. Marotti, E.A. Dalchiele, *Soc. Chil. Quim.* **47**, 1 (2002).
- [39] R. Henríquez, P. Grez, E. Muñoz, H. Gómez, J. A. Badán, R. E. Marotti, E.A. Dalchiele, *Thin Solid Films* **518**, 1774 (2010).
- [40] S. Alamdari, M.J. Tafreshiand, M.S. Ghamsari, *Mater. Lett* **197**, 94 (2017).
- [41] C. Wu, L. Shen, H. Yu, Q. Huang, Y.C. Zhang, *Mater. Res. Bull.***46**, 1107 (2011).
- [42] G. Kaur, A. Mitra, K.L. Yadav, *Progress in Natural Science: Mater. Inter.***25**, 12 (2015).
- [43] A.A. Dakhel, *Microelectron. Reliab.***50**, 211 (2010).